

Review of computational fluid dynamics simulation techniques for direct contact membrane distillation systems containing filament spacers

Amir Bashirzadeh Tabrizi, Binxin Wu*

College of Biosystems Engineering and Food Science, Zhejiang University, China, Tel. +(86) 15896383786;
emails: bwu66@zju.edu.cn (B. Wu), bashirzadeh@hotmail.com (A.B. Tabrizi)

Received 16 September 2018; Accepted 26 April 2019

ABSTRACT

This paper reviews recent research using computational fluid dynamics (CFD) simulations to investigate the hydrodynamics conditions, heat and mass transfer in conventional and newly designed direct contact membrane distillation (DCMD) modules, such as those deploying spacer-filled feed channels. Guidelines and recommendations are presented for computational grids, numerical algorithm and schemes, spatial and temporal discretization, turbulence modelling and computational domain sizes. Most of the work which utilized CFD techniques to study DCMD systems focused on hydrodynamics and heat transfer optimization and investigating the effect of different spacers' geometry, while few of them have tried to achieve a better understanding of the mechanisms resulting in mass transfer enhancement inside the membrane pores. This paper also reviews the different ways in which the CFD simulations are applied to improve performance of the DCMD systems.

Keywords: Direct contact membrane distillation (DCMD); Computational fluid dynamics (CFD); Turbulence models; Heat and mass transfer; Spacer optimization

1. Introduction

In the last two decades, supply and demand for fresh water has increased. Membrane Distillation (MD) is a potential technology for desalting highly saline waters. Membrane Distillation is a separation process which is driven by thermal phenomena, such that only vapor molecules can pass through a porous hydrophobic membrane. This process is operated by the vapor pressure difference between the surfaces of the porous hydrophobic membrane [1,2]. The temperature difference between the feed side of the membrane (T_{mf}) and the permeate side of the membrane (T_{mp}), as shown in Fig. 1, creates different partial pressures of water vapour at the feed (P_{mf}) and the permeate side (P_{mp}). The actual force which is driving the flux through the membrane is the vapor pressure difference. Only the evaporated phase

is transferred across the membrane. Thin membranes can generate large vapor pressure gradients allowing MD to be run at relatively low feed temperatures that potentially can reuse waste heat from other processes [3,4].

MD has many advantages compared to the conventional process. It uses low operating temperatures; it is not necessary to heat up the influent solution (mainly water) to the boiling point. In addition, the hydrostatic pressure applied in MD is lower than that used in membrane processes which are driven by pressure in reverse osmosis (RO). MD can be a cost-effective process, which requires less demanding membrane characteristics as well. So less expensive material can be utilized in MD processes. Based on the principle of vapor-liquid equilibrium, a high rejection factor and complete separation can be provided by using MD. Additionally, the membrane pore size needed for MD processes is relatively

* Corresponding author.

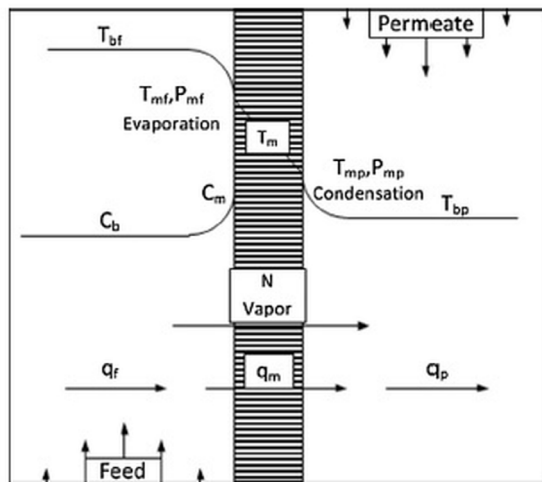


Fig. 1. Operation of direct contact membrane distillation [3].

larger than those for other membrane separation processes. This leads to less fouling problems in MD process experience [1].

The MD systems have the potential to be combined with other separation processes to make an integrated separation system, such as ultrafiltration or with a RO unit [5,6]. Also, MD can utilize renewable energy sources, such as solar energy [7,8]. The MD processes are competitive for brackish water and sea water desalination [9,10]. They are also effective processes for eliminating the organic and heavy metals from aqueous solutions and waste water [11,12]. MD processes have also been applied to treat radioactive waste to discharge the product safely to the environment [13]. However, MD processes suffer from some weak points such as low permeate flux (compared to other separation processes), high sensitivity of permeate flux to the feed temperature and feed concentration caused by temperature and concentration polarization phenomenon. In addition, the trapped air within the membrane generates an extra mass transfer resistance, which can also decrease the MD permeate flux. In MD processes, the heat lost by conduction is somewhat large as well [1].

Different MD configurations such as direct contact membrane distillation (DCMD), air gap membrane distillation, sweeping gas membrane distillation, vacuum membrane distillation etc. have been applied to separate aqueous feed solutions by utilizing a microporous hydrophobic membrane. In DCMD (Fig. 2), the hot feed solution is in direct contact with the hot surface side of the membrane. Therefore, there is evaporation at the feed-membrane surface. The vapor is transported to the permeate side by the pressure difference across the membrane and condenses inside the membrane module. Due to the hydrophobic characteristic of the membrane, the feed solution cannot infiltrate through the membrane (only the gas phase moves inside the membrane pores). DCMD is the simplest configuration form for MD processes, and is widely deployed in desalination processes, aqueous solution concentration for food industry applications and acids manufacturing. The heat lost by conduction is the main weak point of this configuration [14–22].

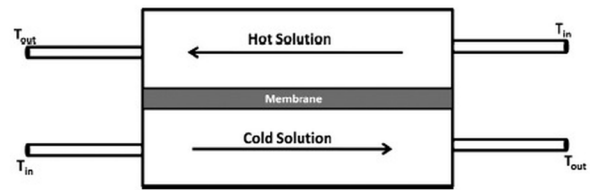


Fig. 2. Direct contact membrane distillation (DCMD) [1].

In the MD process, hydrophobic (non-wetting) microporous membranes are used. Hydrophobic microporous membranes are made from polytetrafluoroethylene, polypropylene or polyvinylidene fluoride. Generally, the membrane deployed in the MD processes should have a low thermal conductivity to prevent heat loss through the membrane and a low resistance to mass transfer. Additionally, the membrane should have a high resistance to chemicals, such as acids and good thermal stability at high temperatures [1]. The thickness of the membrane is an important characteristic in the MD processes. There is an inverse proportional relationship between the thickness of the membrane and flux of permeate. However heat loss is also reduced as the thickness of the membrane is increased. Membranes with pore sizes between 100 nm to 1 μm are usually deployed in MD processes [23,24]. By increasing membrane pore size, the permeate flux increases [24]. The importance of pore size distribution in MD flux has been examined by several investigations [25–29]. Comprehensive understanding of membrane morphology such as pore size, distribution of pore size, porosity, and thickness can help provide an accurate model for heat and mass transfer [24,30–34].

MD can be deployed in many different applications. Although there are some commercial plants that have been recently established to produce fresh water, most of the current MD applications are in a small scale pilot plant phase [35–39].

Traditionally, the semi-empirical models such as Nusselt and Sherwood equations are utilized to predict the temperatures and concentrations at the membrane surfaces. The predicted temperatures and concentrations by using these semi-empirical approaches usually are constant. As these equations are designed for a certain geometry and flow rate regime, the models may not be valid when used for geometry optimizations [3,40]. The understanding of mass transfer in membrane separation systems can be improved by using computational techniques. Computational techniques have the capability to provide information on flow conditions at any point of the geometry without disturbing the flow with sampling and instrumentation. In addition, utilizing numerical modelling can significantly reduce the time, costs, and risks which are associated with performance of repeated experiments [41]. Computational fluid dynamics (CFD) is a branch of fluid mechanics that applies numerical approaches to simulate a fluid flow [42]. The development and application of CFD models began in the early 1950s mainly to solve aeronautic problems. The CFD models can be deployed in terms of virtual geometry prototyping [43]. For MD applications, the CFD models can be applied to predict the temperatures and concentrations

locally throughout the MD module, for MD performance optimization and identification of “performance bottlenecks” as well [3]. In the most recent decade, CFD has been widely used in the field of membrane science as an analysis tool [44]. More and more research groups are applying CFD techniques to gain insight into the phenomena happening inside membrane modules, modify the performance of membrane modules and assist in the design process. In the CFD models the operating conditions, fluid properties, geometric characteristics of the flow channels and membrane modules can be changed in a flexible but defined way. The geometric parameters of the membrane system can be altered without the need to construct and set up a new experiment. This represents a considerable advantage for the CFD techniques compared to traditional experimental methods. Additionally, it is possible to determine flow data at any position and any time during the simulation, and evaluate these flow variables without any disturbance of the actual flow [45–49].

The current paper provides an extensive literature review on the computational fluid dynamic simulation of DCMD systems. Different aspects such as hydrodynamic improvements of the MD channels, heat and mass transfer optimization in the MD channels, mass transfer inside the membrane, improving the flux of the system etc. are reviewed. Several review papers have been published describing modeling and simulation of MD systems but to the best of our knowledge none of them focused on DCMD systems. Moreover, recommendations and guidelines in terms of the spatial and temporal discretization, turbulence modelling, computational domain size and numerical scheme and algorithm are presented in this review which has not been discussed by previous review papers. Also this paper will discuss different turbulence models, their advantages and disadvantages and provide information on creating and performing accurate and reliable CFD simulation of DCMD systems.

1.1. Economics of DCMD systems

The cost of DCMD systems is one of the most important parameters determining the competitiveness of this system compared to other membrane technologies. Similar to other membrane technologies, the cost of an installed DCMD system is dependant on the plant capacity, cost of the energy, feed type, feed quality, pre-treatment, life of the plant, etc. The total cost is categorized as capital cost and operational cost. Capital cost includes equipment purchasing costs, cost of the land and installation costs while operating costs cover operation and maintenance costs, membrane replacement costs, thermal energy costs to heat up the feed solution and the electrical energy cost to run the circulation pumps, vacuum pumps, etc. [50,51]. Table 1 compares the estimation of levelized cost of water for different membrane technologies based on available data from published literatures.

Almost, all the previous studies have introduced the concept of waste heat application to drive MD as the system which makes DCMD systems commercially viable [56]. However, waste heat is not free heat as mentioned by most of the previous studies. Waste heat recovery has a capital cost (heat exchanger, piping, pumps, valves etc.) and operating costs (electricity, maintenance etc.) which should be taken into account as well. Economical evaluation of DCMD process were performed by Al-Obaidani et al. [52] showed that the estimated water cost was $\$1.17 \text{ m}^{-3}$ for DCMD with heat recovery, which was competitive compared to the water cost produced by conventional thermal processes such as multiple effect distillation (MED) and multi-stage flash (MSF) (around $\$1.00 \text{ m}^{-3}$ for MED and $\$1.40 \text{ m}^{-3}$ for MSF). Their evaluation also confirmed that using a low-grade thermal energy source can decrease the cost of the water produced by DCMD to values close to the cost of water produced by RO (about $\$0.50 \text{ m}^{-3}$).

Zuo et al. [57] used Aspen Plus to simulate a DCMD system for economic analyses. Their results showed that

Table 1

Estimation of levelized cost of water (LCOW) for different membrane distillation (MD) systems (direct contact membrane distillation (DCMD), air gap membrane distillation (AGMD), vacuum membrane distillation (VMD), reverse osmosis (RO) combined with different MD systems)

Membrane technology	LCOW ($\$ \text{ m}^{-3}$)	Year	Reference
DCMD (with heat recovery) ^a	1.17	2007	[52]
DCMD – solar	12	2011	[50]
DCMD – waste heat	3.5	2011	[51]
DCMD – waste heat	1.1–1.5	2011	[53]
AGMD – solar	18	2011	[51]
VMD – solar	16	2011	[51]
AGMD – waste heat	5.5	2011	[51]
VMD – waste heat	2	2011	[51]
VMD – steam ^b	0.4–2.4	2016	[54]
RO – MD ^c	1.25	2004	[55]
RO – VMD (steam) ^b	0.6–1.4	2016	[54]

^aCost data from a case where the heat from the brine was considered to preheat the feed water (heat recovery efficiency 80%).

^bRange of estimated water cost is calculated based on the assumed variations in the steam cost and membrane cost.

^cReject brine from RO is used as the feed solution for MD. The estimated cost includes the cost of the entire system.

the lowest water production cost of around $\$1.5 \text{ m}^{-3}$ can be achieved. In addition, the cost of water produced by DCMD system can be reduced further when less expensive waste heat is available. They also found that there was a minimum point of $\$1.1 \text{ m}^{-3}$ for the water production cost when the membrane area was around 4 m^2 . Also, their results indicated that the water production cost decreased gradually by increasing of fluid velocities since the power consumption of fluid pumping has a minor effect on total water production cost for low feed and permeate velocities.

2. Guidelines and recommendations toward reliable and accurate CFD simulation for DCMD processes

This section aims to provide recommendations and guidelines about accurate and reliable CFD simulation of DCMD processes. Appropriate computational grids, numerical algorithm and schemes, spatial and temporal discretization and computational domain size are reviewed.

The computational grid is an important part of any reliable CFD simulation. Improving the convergence rate and computational accuracy can be achieved by applying a high quality grid. A low quality grid may lead to meaningless results or even failure to converge. In general, grids can be categorized as structured and unstructured grids. In structured grids, the grid elements are quadrilaterals for two-dimensional simulation and hexahedra for three-dimensional (3D) simulation. In structured grids, every node is uniquely identified by its indexes but in an unstructured grid, grid points have no particular ordering. The main advantage of structured grids is the linear address space representation of grid point indexes. This advantage provides a very quick and easy access to the neighbours of a grid node. However, it is difficult to develop structured grids for complex geometries [58]. Fig. 3 shows a structured computational grid for a CFD simulation of a DCMD module to study the effect of spacer orientation on the temperature polarization [59].

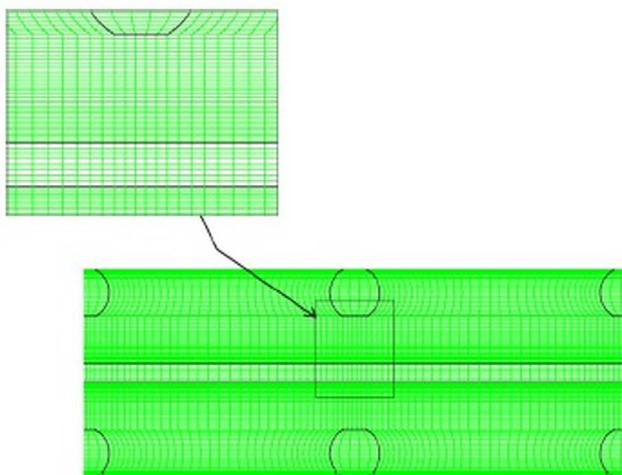


Fig. 3. Structured computational grid for a computational fluid dynamic simulation of direct contact membrane distillation modules [59].

The required resolution of the computational grid depends on the problem. The appropriate grid resolution is usually determined based on the grid independency study. A finer grid provides more accurate numerical results, but it also has a higher computational cost and a larger computer memory requirement. The optimum grid size can be achieved by increasing the grid number until the mesh is sufficiently fine and yet more refinement does not significantly affect the results [59–62].

The grid should be more finely resolved near the wall regions such as membrane, walls of the channels etc., where the velocity gradients are high. The dimensionless wall parameter, y^+ , is a parameter which describes how many cell points should be placed within the wall boundary layer. For any turbulence model, wall function is valid within a specific range of y^+ . The y^+ should be identical to the applied turbulence wall function. The y^+ affiliated with the first cell should not be too large or too small such that the first node is placed outside of the log-law layer or the first node is located in the viscous sublayer of the boundary layer. Fig. 4 shows a finely resolved grid near the membrane for CFD study of a spacer filled flat plate membrane distillation module [59,63–66].

In most of the cases flow can be considered incompressible when simulating DCMD processes and therefore incompressible flow solvers may be employed. Semi-implicit method for pressure linked equations, pressure-implicit with splitting of operators and COUPLED pressure-velocity coupling methods were applied by different researchers [60,63,65,67]. In any CFD simulation, it is necessary to recognize that the solution to discretize governing fluid flow equations converge to a final solution by applying some iterative procedures. There are different methods to check the solution convergence. One method is to test if the residuals of the iterative process for the governing equations are under a certain value. Monitoring an accumulating fluid quantity may result in a constant oscillating trend. The mass conservation (balance) between inlet and outlet normally needs to be verified [43,58].

The time step should be small enough to adequately capture the small-scale turbulent eddies of transient flow. Shakaib et al. [59] mentioned that when the Reynolds number is high and exceeds a certain critical value, the flow becomes transient and time dependent. Schwinge et al. [68] applied time steps of $5 \times 10^{-6} \text{ s}$ for the transient mode and achieved convergence within a maximum of 20 iterations for each step in a CFD study of unsteady flow in narrow spacer-filled channels for spiral-wound membrane modules. Cao et al. performed transient simulations with a fixed time step of $2 \times 10^{-3} \text{ s}$ as part of CFD simulations of net-type turbulence promoters in a narrow channel [69]. Cipollina et al. [70] set a time step of $5 \times 10^{-4} \text{ s}$ for a transient simulation in a CFD simulation of a membrane distillation module channel to keep the Courant number below 1.

The size of the computational domain should be large enough to minimize the uncertainties of the boundary conditions on the results. However, it should not be too large to unnecessarily raise the number of elements and increase computational time. Fig. 5 schematically shows the computational domain setup representing a channel section of the tubular membrane with a length of 100 mm

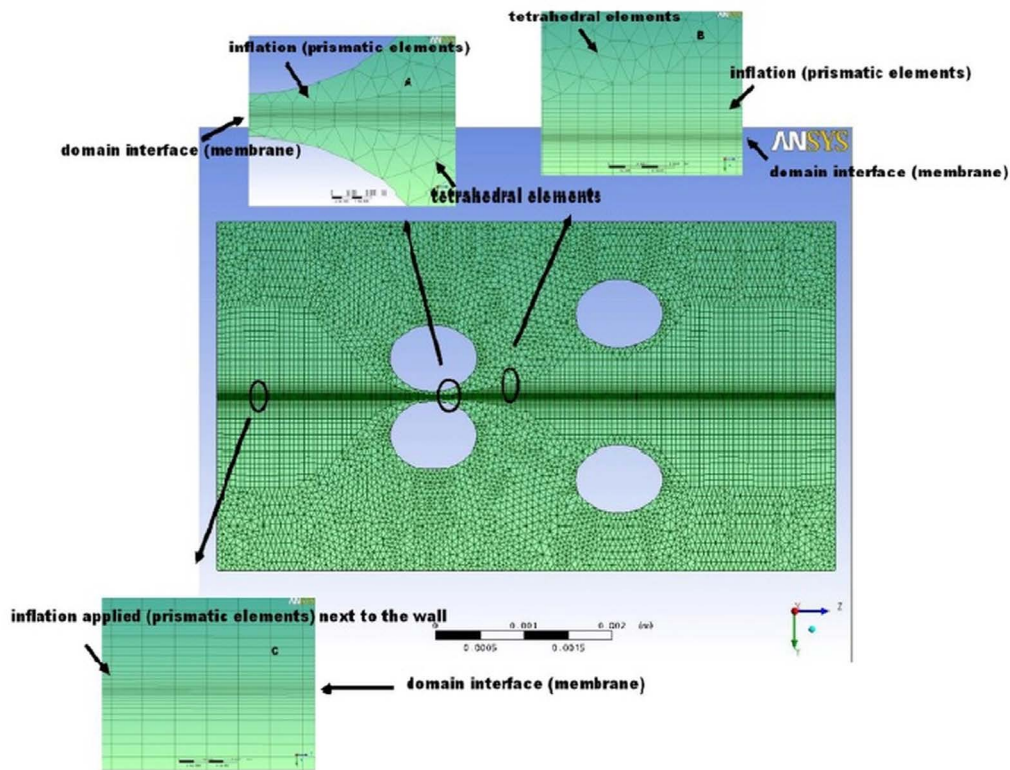


Fig. 4. Finely resolved grids near the membrane [63].

and a height of 2.5 mm for CFD simulation of MD of a NaCl solution [65].

3. Applications of different turbulence models for the DCMD process

This section reviews different approaches to model turbulent flows in DCMD systems. Advantages and disadvantages of different turbulence models such as $k-\epsilon$, $k-\omega$ shear stress transport (SST), SST transition, large eddy simulation (LES), and hybrid Reynolds averaged Navier-Stokes (RANS-LES) are considered.

3.1. $k-\epsilon$ turbulence model

The $k-\epsilon$ turbulence model solves two transport equations for turbulent kinetic energy, k , and turbulent dissipation rate, ϵ , to calculate the eddy viscosity in the RANS equations. This model is stable, economic and reasonably accurate, which is why it is so widely used in industrial flow field and heat transfer simulations. The standard $k-\epsilon$ model has

become the main tool for engineering flow field calculations since it was developed. It is a semi-empirical model that is based on experimental phenomena. The turbulent kinetic energy transport equation is derived from the exact equation and the dissipation rate equation is derived from the physical inference and the mathematical simulation of a similar prototype equation. By solving the turbulent kinetic energy equation and the turbulent dissipation rate equation, the standard $k-\epsilon$ model obtains the solutions of k and ϵ , then calculates the turbulent viscosity by using the values of k and ϵ , and finally obtains the solution of Reynolds stress using the Boussinesq hypothesis. The standard $k-\epsilon$ model assumes that the flow is completely turbulent, and the influence of molecular viscosity can be neglected. This model is only suitable for the simulation of the flow processes experiencing complete turbulence [58,71].

Several improved $k-\epsilon$ models such as renormalization group (RNG) $k-\epsilon$ model and realizable $k-\epsilon$ model have been developed. The RNG $k-\epsilon$ model is derived from strict statistical techniques. It is similar to the standard $k-\epsilon$ model but improved by: adding a condition to the ϵ equation to

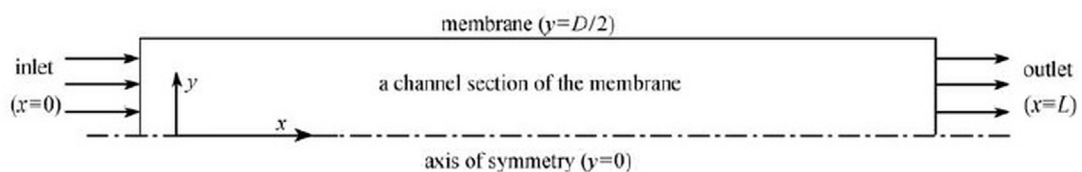


Fig. 5. Computational domain setup representing a channel section of the tubular membrane [65].

improve the accuracy of the model and taking the turbulence swirl into account to effectively improve the accuracy. The standard $k-\epsilon$ model is a high Reynolds number model. The RNG theory provides an analytical formula for considering the viscosity of low Reynolds number flows. The function of these formulas depends on the correct treatment of the near-wall region. These characteristics make the RNG $k-\epsilon$ model more reliable and accurate than the standard $k-\epsilon$ model for a wide range of flows [72,73].

The realizable $k-\epsilon$ model has two major differences compared to the standard $k-\epsilon$ model: (i) the realizable $k-\epsilon$ model adds a formula for turbulent viscosity and (ii) a new transmission equation is added to the dissipation rate, which is derived from an exact equation for laminar velocity fluctuations. The term "realizable" means that the model must ensure mathematical constraints and continuity of turbulence under Reynolds pressure. The direct advantage of the realizable $k-\epsilon$ model is a more accurate prediction of the divergence ratio between flat and cylindrical jets. It has good performance for rotating flows, inverse pressure gradient boundary layer flows, flow separation and secondary flows [71,74].

The realizable $k-\epsilon$ model and the RNG $k-\epsilon$ model perform better than the standard $k-\epsilon$ model when there is sharp streamline bending, and in whirlpool and rotational flows. Initial research shows that the realizable $k-\epsilon$ is more accurate in flow separation and secondary flows among all the $k-\epsilon$ models. The realizable $k-\epsilon$ model is suitable for many different flow types, including swirling uniform shear flow, free flow (jet and mixing layer), channel flow and boundary layer flow. The simulation results of these flow processes are better than those using the standard $k-\epsilon$ model, especially in the simulation of circular jets and flat jets [71,75]. One drawback of the realizable $k-\epsilon$ model is that it cannot provide the natural turbulent viscosity when calculating the rotating and static flow regions [71].

3.2. $k-\omega$ (SST) turbulence model

The $k-\omega$ (SST) turbulence model is a blend between $k-\epsilon$ and $k-\omega$ turbulence models. It employs the $k-\omega$ turbulence model for the inner sector of the boundary layer and gradually transitions to the standard $k-\epsilon$ turbulence model in the wake zone of the boundary layer and free shear layers [76]. A blending function is applied to make the transition between these two models. This blending function has a value of one in the sublayer and logarithmic zone of the boundary layer and then gradually moves to zero in the wake zone and free shear layers. The other advantage of the $k-\omega$ (SST) turbulence model is that the eddy viscosity formulation is improved to take into account the turbulent SST effect. This turbulent SST is important when flow with a severe adverse pressure gradient is simulated [77].

3.3. SST transition turbulence model

The basic principal of the SST transition turbulence model is the coupling of the $k-\omega$ (SST) transport equations with two other transport equations which apply the intermittency and the transition momentum thickness Reynolds number. The SST transition turbulence model can predict flow separation phenomena and provide more accurate results compared to the classical fully turbulent models [77,78].

3.4. Large eddy simulation

In LES, large eddies are solved directly, and small eddies are simulated with a sub-grid scale model. A main function of the small eddies is to dissipate the turbulent energy which is transferred from the larger scales to the smaller scales by an energy cascade [79].

In the LES method, a low-pass spatial filtering of the governing equations is used to achieve the separation between the resolved and unresolved scales. The subgrid-scale stresses which results from the filtering operation are uncertain, and need to be modelled [80]. The approach is a compromise solution between direct numerical simulation (DNS) and RANS. All scales are numerically solved in DNS, while in RANS, all scales are modelled. In LES, the transport equations are filtered such that only larger eddies are resolved and the smaller eddies are modelled. Therefore, LES is an efficient method of achieving good results in turbulent flows [78]. As LES requires that only larger eddies resolve, a coarser mesh and a larger time step can be applied compared to DNS, but still a much finer mesh is needed compared to other turbulent models. LES has to run for a long flow-time to obtain statistics so that the flow can be modelled and achieve good results. As a result, computational costs in terms of random access memory and central processing unit are higher than RANS models and high-performance computing is required [81].

3.5. Hybrid RANS-LES turbulence model

The hybrid RANS-LES turbulence model is a mixed method of the statistical RANS and LES techniques. The basic rule in the hybrid technique is applying RANS to solve the boundary layer, while LES is deployed for the external flow and separation regions. This method reduces the computational demands of LES and provides more accuracy compared to the RANS [77,78].

As mentioned in section 3.1, the $k-\epsilon$ model is popular when simulating a broad range of turbulent flow and heat transfer processes. Most of the researchers who simulated DCMD processes with CFD applied the $k-\epsilon$ turbulence model to model turbulent flows. For example, Ranade and Kumar [47,82] used the standard $k-\epsilon$ turbulence model to compare the flow in a spacer-filled flat channel with a curvilinear channel. However, Shakaib et al. [67] mentioned that the standard $k-\epsilon$ turbulence model performed poorly when applied to simulate flows in narrow spacer-filled channels. Yang et al. [60,83] deployed a realizable $k-\epsilon$ method to simulate turbulent conditions, analyze the effect of turbulence promoters in hollow fiber membrane distillation modules and optimize micro-structured hollow fiber design for MD applications. Karode and Kumar [46] employed the RNG $k-\epsilon$ model to visualize flow through spacer filled channels with a CFD simulation. Cao et al. [69] used the RNG $k-\epsilon$ turbulence model to simulate net-type turbulence promoters in a narrow channel.

4. Different applications of CFD in DCMD process

This section is divided into three parts. The models discussed in section 4.1 are focusing on improving the hydrodynamics and heat transfer in the channels of DCMD

modules. The models in section 4.2 investigate improving the flux of the DCMD systems and the models in section 4.3 focus on spacer optimization in DCMD systems.

4.1. Improving the hydrodynamics and heat transfer in the channels of DCMD modules

The CFD models discussed in this section focus on analyzing and improving hydrodynamics and heat transfer conditions in the DCMD module channels.

Shakaib et al. [84] used CFD modelling to examine transient flow and temperature patterns in spacer-filled membrane distillation channels. The instantaneous velocity profiles which developed at various time steps showed that for a higher Reynolds number, the vortices appear behind the spacer filaments, then move along with the flow and then finally disappear. This unsteady behavior varies with time depending on local temperatures and heat transfer coefficients. They found that the temperature polarization is usually low near the places where a high velocity region is adjacent to the top or the bottom surface. Their results also show that there is a stagnant zone and an area of higher temperature polarization in the region near the filament at the bottom. They obtained maximum values for average shear stresses and heat transfer coefficients at low Reynolds numbers and a small filament spacing of 2 mm, while for high Reynolds numbers these spacers are unsuitable.

Al-Sharif et al. [61] developed a three-dimensional model by using the open source CFD package Open Foam. Three types of spacers (90°, 45° and 3 layer double ladder shaped non-woven spacers) were modelled and a constant heat flux through the membrane in a single channel was applied as an assumption. As a reference, they compared the profiles of velocity magnitude and temperature averaged over 9 sampling points against published results for corresponding cases [85]. Generally, they observed good agreement in predicted velocity profiles while there were some differences in temperature profiles between the two data sets. They explained that the heat loss at the membrane surfaces resulted from the temperature decreasing along the direction of the flow and as a result the temperature profiles are sensitive to location along that direction. They believed that the differences in temperature profiles between the two data sets are due to differences in the locations of the sampling points used for averaging. Their results emphasised that the 3 layer, double ladder spacer improves the heat transfer and is the best performing spacer with the least pressure drop. The authors mentioned that this good performance is due to the flow being forced to go around the middle filament and towards the membrane. Fig. 6 shows the flow in the wake region of the transverse filaments of spacer type 2 and Fig. 7 displays the temperature and flow of spacer type 3.

Cipollina et al. [70] performed a study on the effects of spacer and channel geometry to reduce temperature polarization by deploying CFD techniques. They built simple reference geometry to model the flow and temperature fields of a portion of a spiral wound MD module channel. Their results displayed how spacers can significantly affect temperature gradients within the channel, and modify the effective driving force between the faces of the membrane.

In another work Shakaib et al. [59] used the commercial CFD software Fluent to develop a two-dimensional CFD model. The model included two channels (feed and permeate) that were flowing around a single flat sheet membrane in a counter current set up. They set the thermal conductivity of the membrane material to a constant value of $0.2 \text{ W m}^{-2} \text{ K}^{-1}$ and included the conductive heat transfer of the spacer material in the calculation. They investigated different 90° spacer arrangements with the spacer filaments adjacent to the membrane, away from the membrane and a staggered (alternating) configuration. The spacer performance for each different arrangement was assessed based on the coefficient of temperature polarization and the pressure drop in the channels. They examined the effect of spacer orientation, inlet velocity and filament spacing on the shear stress distribution and temperature polarization in the MD modules. The Nusselt numbers for the three in-line orientations AI, BI and CI (Fig. 9) computed from the simulation were compared to those obtained in the experimental works performed by Phattaranawik et al. and Shirazi et al. [86,87]. Since the correlation was developed from experiments considered valid only in the Re range of 400–1,000, the simulated Nu values were obtained only for velocities (0.25 and 0.35 m s^{-1}) which fall in the same Re range. The simulated Nu values were in close agreement with the ones obtained from the experimental correlation. Their CFD simulations showed

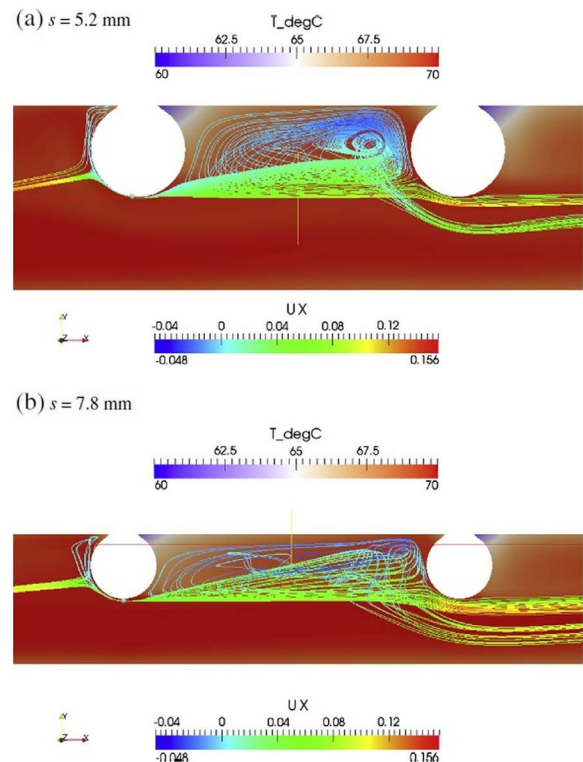


Fig. 6. Flow in the wake region of the transverse filaments of spacer type 2. Stream tracers originate from a line source near the bottom of the left filament (integration backwards and forwards from the line source), and are colored by the x -component of velocity. The background temperature color-map clearly shows the lower temperatures in the stagnant regions behind the filaments [61].

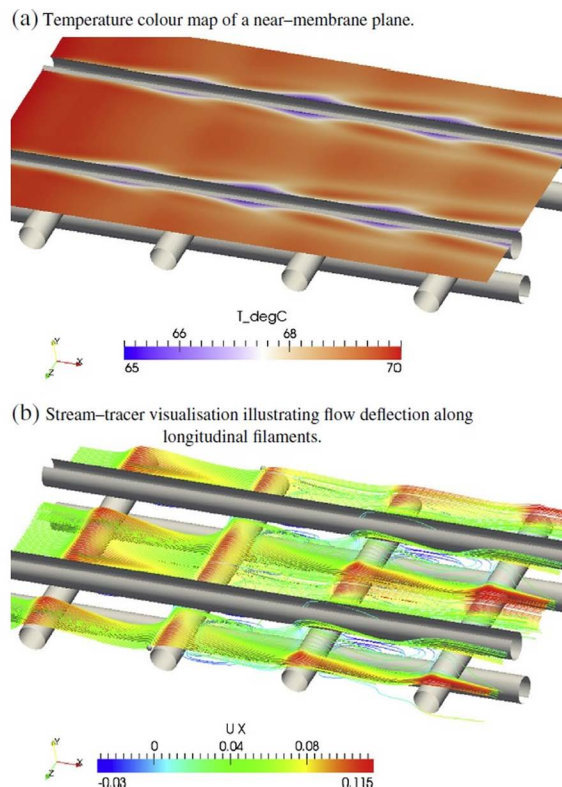


Fig. 7. Temperature and flow of spacer type 3 illustrating the cool spots on the sides of the longitudinal filaments in the region between transverse filaments and the flow pattern that causes the cool spots to occur [61].

that the spacer orientation alters the temperature polarization and heat transfer rates. The temperature polarization is high in the arrangement where spacer filaments touch the top or bottom surfaces of the membrane, which results in lower heat transfer rates. Temperature polarization is lower in the configuration where the filaments are detached from the membrane. Also in the detached mode, the shear stress is higher and local values of temperature polarization index and shear stress are distributed more uniformly. They mentioned that the detached orientation is more favorable for use in MD modules. Fig. 8 shows the nomenclature of spacer orientations which they considered in their work. Velocity and temperature distributions in different spacer types are displayed in Fig. 9.

4.2. Improving of the flux of the DCMD systems

In this section, the CFD models discussed are used to analyze and improve the flux of the DCMD systems.

Yu and his team [88] performed a comprehensive analysis on the dominant effects of heat and mass transfer in the DCMD process by using CFD simulations. They used two hollow fiber modules (a single fiber MD module with an effective fiber length of 0.25 m and a membrane area of 0.0011 m²), either baffled or non-baffled, to investigate the heat and mass transfers during DCMD processes. They recirculated the feed and distillate streams through the

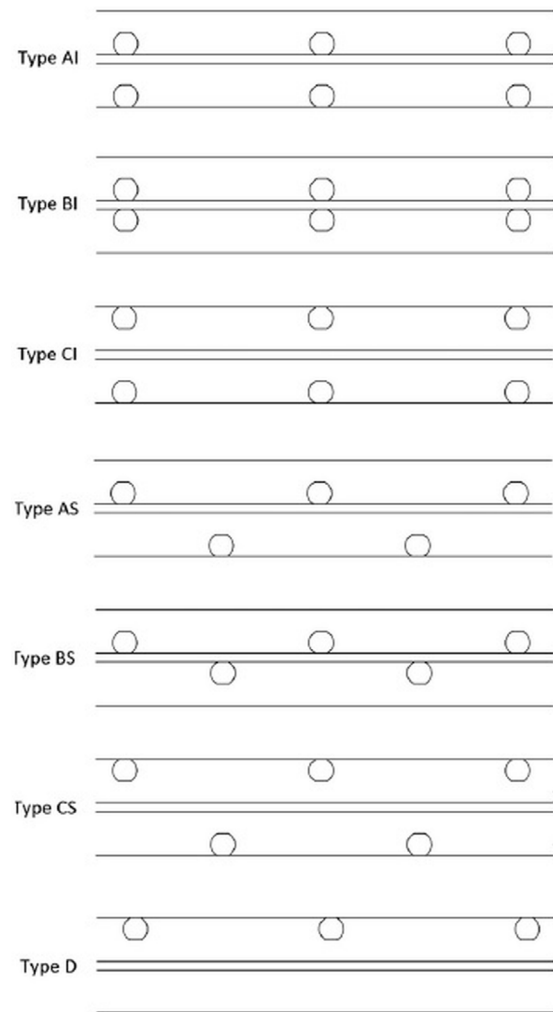


Fig. 8. Nomenclature of spacer orientations considered by Shakaib et al. [59].

hollow fiber module in counter-current mode. They fed the hot stream (simulated seawater: 3.5 wt.% NaCl solution) through the shell side and the cooled distillate stream (pure water) was recirculated on the lumen side. They performed numerical simulations to study the effect of the MD intrinsic mass transfer coefficient of the membrane to enhance the performance in both baffled and non-baffled modules. They investigated potential enhancement strategies under different circumstances. They conducted five sets of temperature variation experimental tests to verify their CFD simulations. Then the simulated mass fluxes from CFD simulations were compared with the experimental results. They confirmed that the simulation data agrees very well with the experimental values. The relative errors were within $\pm 5\%$, which confirmed the reliability of their simulations. Their results showed that increasing the intrinsic mass transfer coefficient value regardless of the existence of baffles decreases the temperature polarization coefficient. In addition, they obtained results showing that increasing the operating temperature decreases the temperature polarization coefficient in the presence of a baffle. The authors mentioned

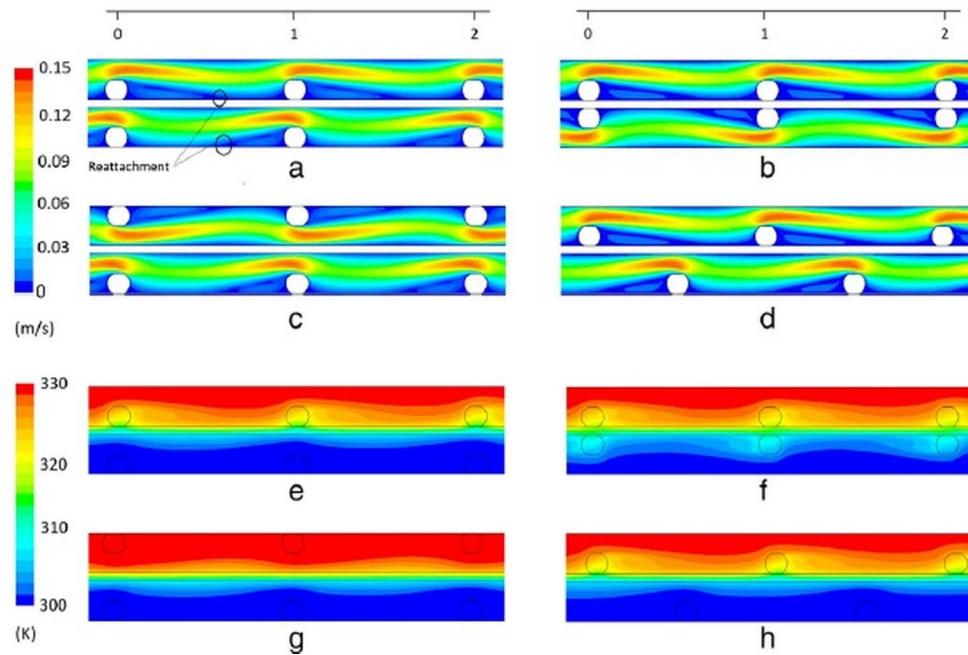


Fig. 9. Velocity and temperature distributions in spacer types AI (a, e), BI (b, f), CI (c, g) and AS (d, h) [59].

that raising the operating temperature had more effect on increasing the mass flux compared to application of baffles. Moreover, they concluded that the higher operating temperatures are more preferable since that improves the mass/heat transfer as well as MD thermal efficiency, even with a smaller temperature difference. Fig. 10 shows the transmembrane mass flux distribution along the module length for non-baffled and baffled modules. Economically the results of the study carried out by Seo et al. [89] for a spacer optimization strategy for DCMD systems indicated that where relatively expensive heat sources were deployed, a symmetric circular-zigzag spacer pattern with a relatively large diameter size and a greater number of filaments was economically viable to maximize vapor flux despite an increased hydraulic pressure drop. In contrast, a symmetric circular-zigzag spacer pattern including a relatively small diameter size and fewer numbers of filaments was economical to minimize the hydraulic pressure drop, where cost-free heat sources were available.

It is notable that the most common module recently deployed for MD experiments is the hollow fiber configuration [90]. With a hollow fiber configuration the membrane can be backwashed and as a result extensive pre-treatment processes are not needed. This is the most important advantage of a hollow fiber configuration when using MD-based desalination and water/wastewater treatment [91].

Comparison between the works conducted by Shakaib et al. [59] and Yu et al. [88], shows that spacers are more effective at reducing the polarizations' effect. Therefore it can be concluded that spacer-filled MD modules are more efficient than that of baffled modules [92]. However, it should be noted that when seawater is used as a feed, applying the spacers can increase the risk of micro-organisms growing and biofouling/fouling which can decrease the distillate flux and cause other problems [93–97]. In this

regard, CFD simulation can be integrated with other simulation techniques such as molecular dynamics [98,99], pore-network [100], or other methods [101,102] for further investigation.

Yang et al. [60] investigated the effect of the microstructure of hollow fibers on the DCMD's performance. They explored the potential of micro-structured hollow fiber designs to enhance the performance of a DCMD system by developing a series of three-dimensional CFD simulations. They investigated hollow fibers with 10 different geometries (wavy and gear shaped cross sections) presented in Fig. 11. For their CFD simulations, they applied a heat-transfer model which was been verified previously based on an established DCMD system for a series of experimental settings [66,83,88]. Based on the previous verification results, they confirmed that there is a good agreement with small relative errors of $\pm 5\%$ between their CFD simulation results and experimental data of mass flux (N_m) and feed pressure drop (ΔP_f). The results showed that for the wavy fiber shape (design No. 07) the heat transfer coefficients were increased up to 4.5-fold while for the gear shape, there is an increase of approximately 5.5-fold. Their results also show that the average mass flux (i.e. N_m) and temperature polarization coefficient of the gear shaped fiber module was enhanced 66% and 57%, respectively compared to the original straight fiber design. It is notable that the enhancement of the MD performance resulted from the improvement of the hydrodynamic condition of the flow over the various fiber geometries. In fact, the performance improvement of the modified fibers was because of the intense secondary flows and surface renewal improvement due to the presence of corrugations on the membrane surface. Moreover, at an extremely low Reynolds numbers their results showed a promising enhancement by the gear-shaped fibers. The authors mentioned that although a flow

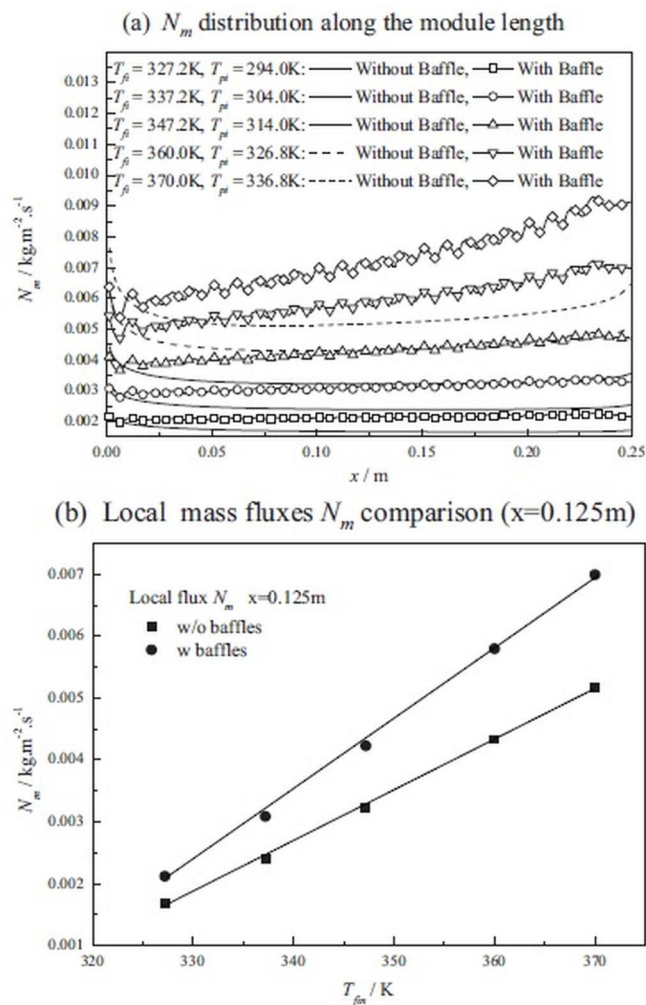


Fig. 10. Transmembrane mass flux (N_m) distribution along the module length for non-baffled and baffled modules at ΔT_{in} (a) N_m distribution along the module length and (b) local mass fluxes N_m comparison $x = 0.125 m$ ($\Delta T_{in} = 33.2 K$, $u_{fi} = 0.06 m s^{-1}$, $u_{pi} = 0.417 m s^{-1}$, $C = 2.0 \times 10^{-7} kg m^{-2} s^{-1} Pa^{-1}$) [88].

transition from laminar to turbulent conditions can make a significant improvement for conventional MD modules, applying smart micro-structured designs into the membrane surface would be a cost effective option for adverse flow conditions. Fig. 12 shows the mass flux distribution along the fiber length for single-fiber modules with fibers of various geometries.

4.3. Optimization of spacer performance in DCMD systems

Several researchers applied CFD models to analyze spacer filled MD modules, the effect of turbulence promoters (spacers) in MD modules and to optimize the spacer performance in DCMD systems.

Katsandri [63,64] used ANSYS CFX to develop a 3D CFD model that describes fluid flow through spacer filled channels on a flat plate DCMD unit. He studied the effect of different hydrodynamic angles on the velocity profiles and shear stress. Also, he investigated how different inlet

velocities and temperatures affect mass flux and temperature polarization. Three hydrodynamic angles, $\alpha_f = 45^\circ$, $\alpha_f = 90^\circ$ and $\alpha_f = 0^\circ$, were simulated by Katsandri. To validate his CFD simulations, he compared CFD results with experimental data obtained from a flat plate membrane distillation module [103]. The Nusselt numbers calculated by the CFD simulations were compared to Nusselt numbers obtained from the experimental data. He confirmed that his model can predict the experimental Nusselt number with a relative error $<11\%$. His results showed that the optimal configuration is when the hydrodynamic angle $\alpha_f = 45^\circ$ as it produces better mixing, increases shear stress resulting in higher fluxes, and results in the highest mid-membrane temperature and temperature polarization coefficient. He concluded that the least desirable configuration is when the hydrodynamic angle $\alpha_f = 0^\circ$, as this produces the lowest mid-membrane temperature and lowest temperature polarization coefficient. Fig. 13 shows the temperature distribution for $u_{eff} = 0.135 m s^{-1}$ in the different unit cell locations for $\alpha_f = 45^\circ$.

Yang et al. [83] modelled nine modified hollow fiber modules with various turbulence promoters (spacers) by using a two-dimensional CFD model to investigate their potential impact on heat transfer and module performance for a shell-side feed DCMD system. They experimentally tested an original and two modified 0.25 mm modules (with annular quad spacers inserted) to verify their CFD simulations for altered configurations and varied flow velocities. The CFD simulation results and experimental data of mass flux and pressure drop were compared. The simulation results agreed very well with the experimental data. The relative errors were within $\pm 5\%$ for both mass flux and pressure drop results. Applying the turbulence promoters resulted in slower decreasing trends along the fiber length for the feed heat-transfer coefficient (h_f) of the modified module compared to the original (unmodified) module. The results showed a 6-fold h_f enhancement with a modified module consisting of annular baffles and floating round spacers. In addition, the temperature polarization coefficient and mass flux of these modified modules increased 57% and 74%, respectively. The temperature profiles and local flow fields obtained from their CFD simulations confirmed that the intense secondary flows and radial mixing can be promoted to improve the shell-side hydrodynamics and enhance heat transfer by using appropriate turbulence promoters. In addition, the authors mentioned that a well-designed module can significantly enhance liquid-boundary layers which dominates heat-transfer process. Moreover, the attached quad spacers or floating round spacers can provide a good compromise between enhanced permeation fluxes and modest hydraulic energy consumption. Fig. 14 shows the local flow field visualization for modules with various turbulence promoters and Fig. 15 shows the mass flux distribution along the fiber length for modules with various turbulence promoters.

Karode and Kumar [46] carried out CFD simulations of fluid flow through rectangular channels filled with several commercially available spacers for flat sheet geometry membrane modules to calculate pressure drop and shear rate. They compared their simulation results with literature experimental data and found excellent agreement between the experimentally determined dependence of the total

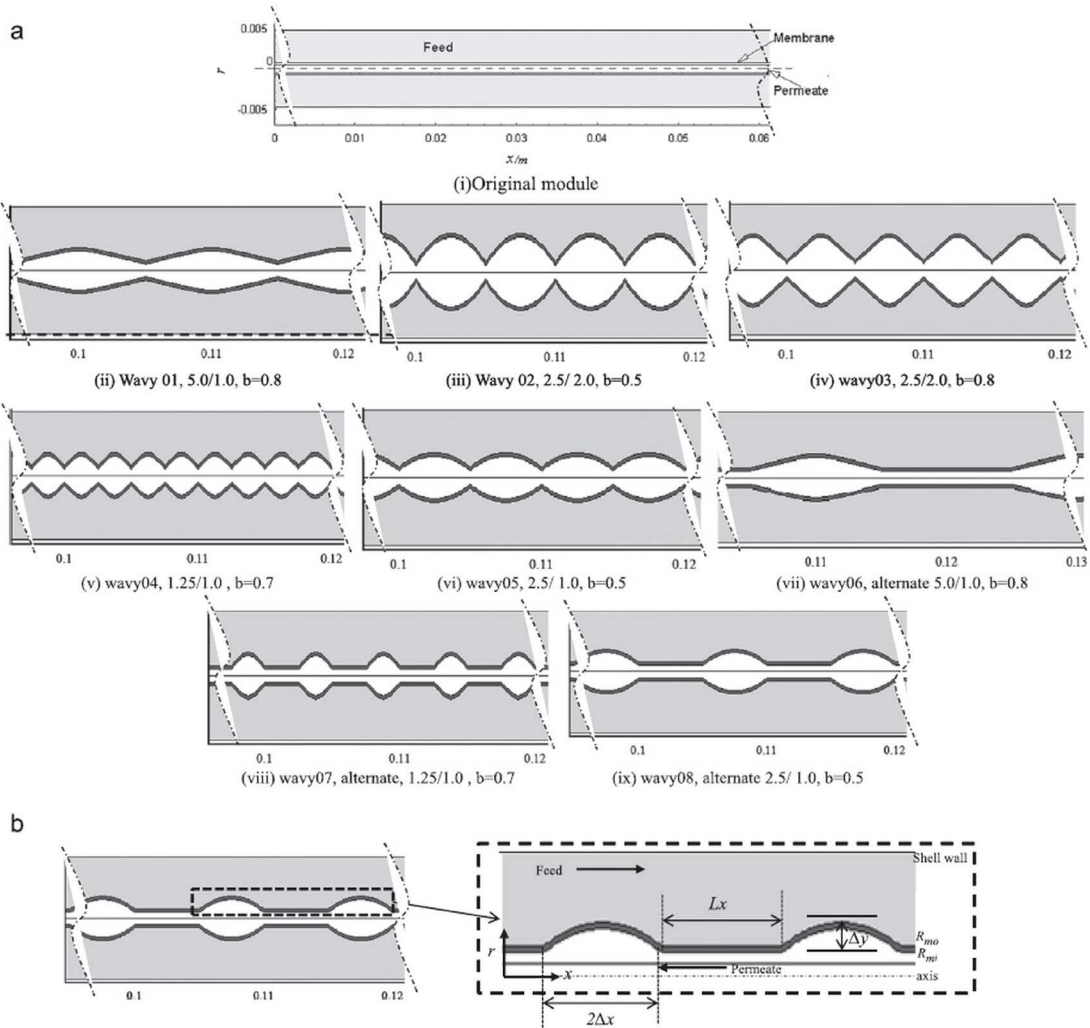


Fig. 11. (a) Schematic of axially symmetric single fiber modules in CFD simulating domains and (b) local domain amplification of an axially symmetric wavy single-fiber module in CFD simulations [60].

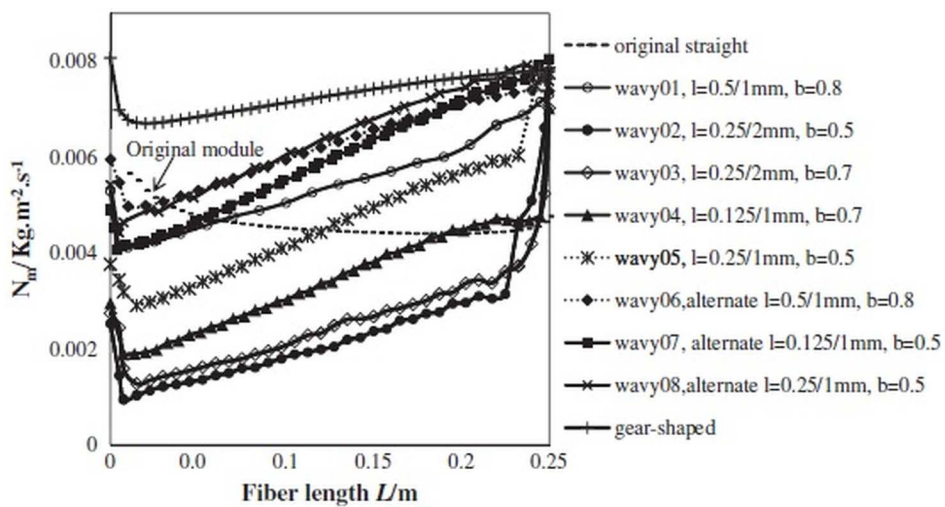


Fig. 12. Mass flux N_m distribution along the fiber length for single-fiber modules with various fiber geometries ($C = 8.0 \times 10^{-7} \text{ kg m}^{-2} \text{ s}^{-1} \text{ Pa}^{-1}$ and $C(\text{gear}) = 6.4 \times 10^{-7} \text{ kg m}^{-2} \text{ s}^{-1} \text{ Pa}^{-1}$, $L = 0.25 \text{ m}$, $T_{fi} = 327.15 \text{ K}$, $T_{pi} = 293.85 \text{ K}$, $u_{fi} = 0.06 \text{ ms}^{-1}$, $u_{pi} = 0.417 \text{ ms}^{-1}$) [60].

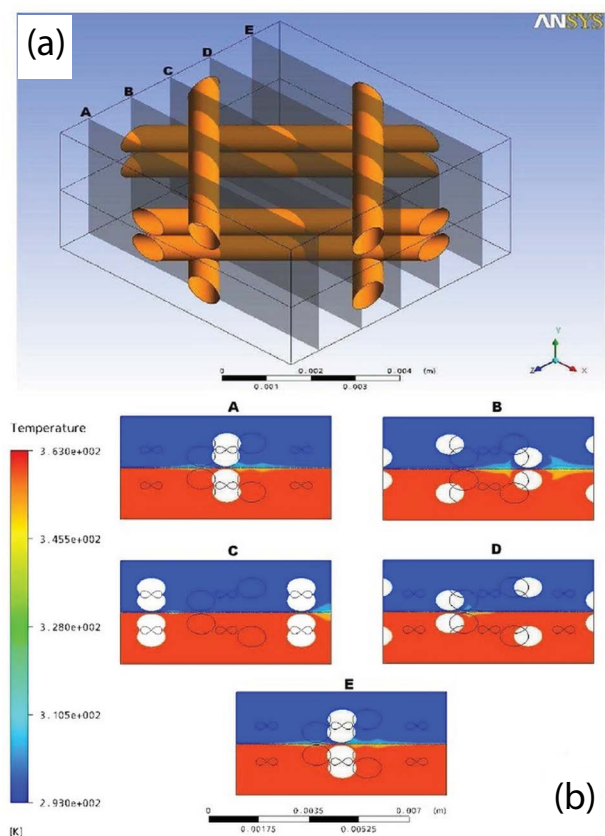


Fig. 13. (a) Marked locations at different positions in the unit cell (45°) and (b) Temperature distribution for $u_{\text{eff}} = 0.135 \text{ ms}^{-1}$ in the different unit cell locations identified in Fig. 13a. (Temperature in K, $\alpha_f = 45^\circ$) [64].

drag coefficient on the Reynolds number and their CFD simulations. Also, at low inlet velocities ($<0.5 \text{ m s}^{-1}$) there was good agreement between the pressure drop predicted by their CFD work and the data experimentally measured by Da Costa et al. [104]. However, for higher inlet velocities their CFD simulation results for pressure drop over predicted compared to the experimental data published by Da Costa et al. [104]. They observed that spacers with equal filament diameters produce a higher pressure drop across the channel and these symmetric spacers also cause a more uniform shear rate at the top and bottom faces of the test cell. Spacers with unequal filament diameters (asymmetric spacers) generated a lower pressure drop and also resulted in an unequal shear rate on the top and bottom faces of the test cell. The authors explained that such unequal shear rates at the top and bottom faces can have an adverse impact on the performance of the membrane module due to different mass transfer characteristics for adjacent membrane leaves.

Applications, assumptions, utilized software, accuracy and finding results of the CFD models reviewed in section 4 have been summarised in Table 2.

5. Modelling of the membrane

There are some challenges in modelling the membranes by CFD approaches. Some of the physical phenomena which

happen inside the membrane such as the surface diffusion have been ignored in most of the CFD simulation which can be important when studying membrane synthesis. In this section, some models and methods of modelling of the membranes that were previously suggested, investigated, and modified by other researchers are discussed briefly.

Srisurichan et al. [105] investigated the mechanism of mass transfer across the membrane and studied the fouling phenomena and its effect on the transport resistances in DCMD process. They applied a mass transfer model based on the Dusty gas model to fit the flux data. Also, the pressure blocking filtration laws were deployed to explain the membrane fouling. The Dusty gas model is often used to predict water flux in MD, where four mass transfer mechanisms (surface diffusion, Knudsen diffusion, molecular diffusion, and viscous flow) may occur; the complete expression of the Dusty gas model is complex, thus surface diffusion, which only exists when membrane pore sizes are smaller than $0.02 \mu\text{m}$ is typically ignored to simplify MD flux prediction [23,27,29]. The results presented by Srisurichan et al. [105] showed that molecular diffusion was the most suitable model for predicting fluxes of both laminar and turbulent flow and a cake filtration model can describe fouling of the membrane by humic acid agglomeration.

Rao et al. [106] developed a simplified water flux prediction model to calculate the water flux of DCMD membranes. The model deployed a new structural parameter that does not contain coupled properties and can be measured independently while still keeping the physical meaning of a relationship with the membrane properties which affect water flux (thickness and porosity). In comparison with the simplified Dusty gas model, the suggested empirical model using C_m has the following advantages: by deploying uncoupled membrane properties, the model can quantitatively analyze water flux with a less complicated expression; the model can be applied for membranes with a wide range of pore sizes ($0.1\text{--}0.9 \mu\text{m}$), predicts flux better and C_m characterization can be performed through simple and reliable measurements. However, deploying C_m for flux prediction has some limitations. It may not be valid for membranes with low porosities and it cannot satisfactory predict water flux for composite membranes when using the linear regression approach.

Imdakh and Matsuura [29] developed a Monte Carlo simulation model to analyze vapor permeation through membrane pores in association with DCMD. In their simulation, a three-dimensional network of interconnected cylindrical pores with a pore size distribution represents porous membrane. Their model took into account at the pore level all molecular transport mechanisms based on the kinetic gas theory and all boundary conditions that may affect DCMD process. They showed that the results obtained from the model are in good qualitative agreement with the available experimental data [107].

Haddadi et al. [108] introduced a new algorithm for CFD modelling of membrane separation. Their suggested algorithm was based on a multi-region approach. The algorithm included a generic platform for implementation of different mass transfer models which made it capable of covering modelling of the trans-membrane flux between retentate and permeates for multi-component separation. It

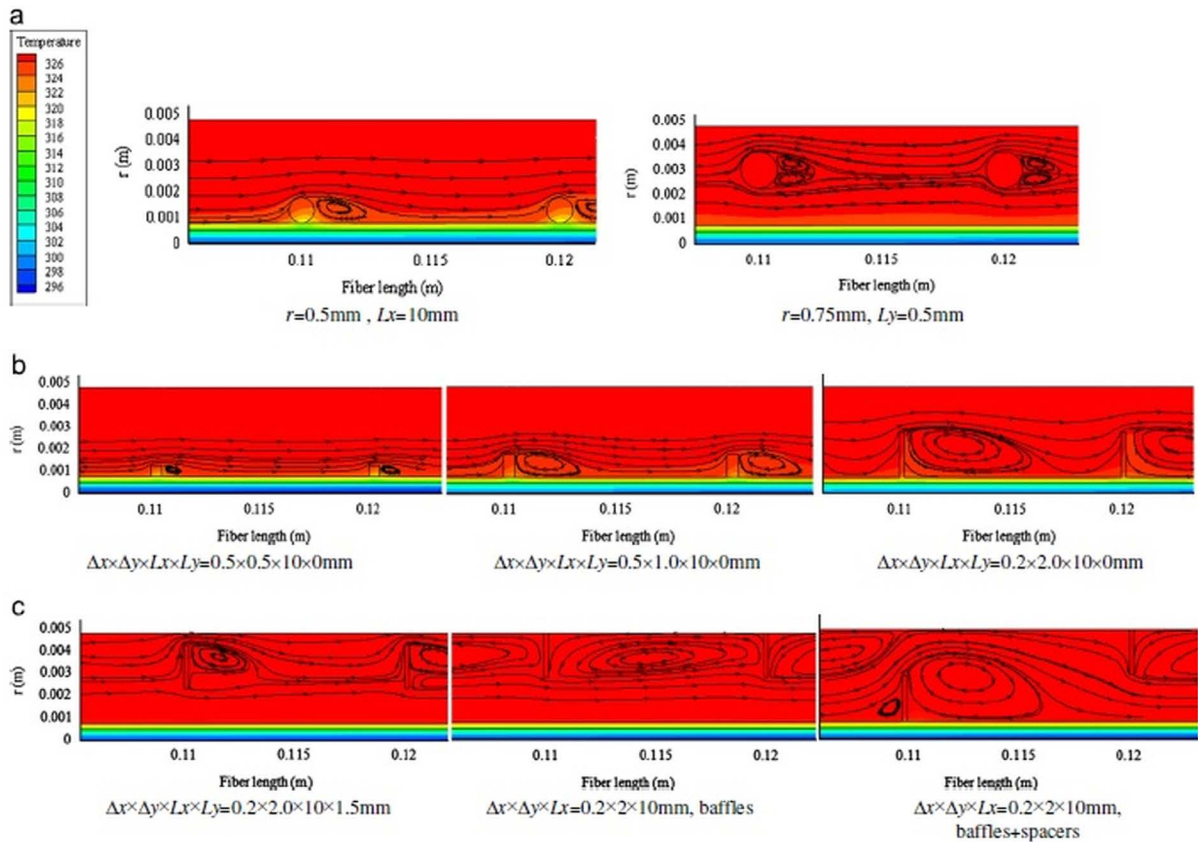


Fig. 14. Local flow fields for modules with various turbulence promoters ($C = 8.0 \times 10^{-7} \text{ kg m}^{-2} \text{ s}^{-1} \text{ Pa}^{-1}$, $L = 0.25 \text{ m}$, $u_{fi} = 0.06 \text{ ms}^{-1}$, $u_{pi} = 0.417 \text{ ms}^{-1}$, $T_{fi} = 327.15 \text{ K}$, $T_{pi} = 293.85 \text{ K}$) [83].

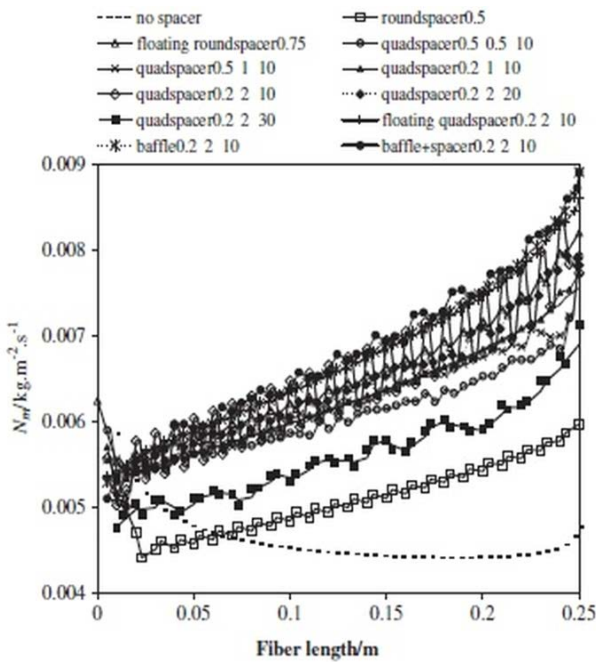


Fig. 15. Mass flux N_m distribution along the fiber length for modules with turbulence aids of various specifications ($C = 8.0 \times 10^{-7} \text{ kg m}^{-2} \text{ s}^{-1} \text{ Pa}^{-1}$, $L = 0.25 \text{ m}$, $u_{fi} = 0.06 \text{ ms}^{-1}$, $u_{pi} = 0.417 \text{ ms}^{-1}$, $T_{fi} = 327.15 \text{ K}$, $T_{pi} = 293.85 \text{ K}$) [83].

also contained generic per-region turbulence modelling and the ability to switch between one-dimensional (1D) and full detail 3D membrane modelling. They implemented the suggested algorithm in the open source platform OpenFOAM. They compared simulation results with experimental data from pure gas permeation of a hollow fiber module and showed that the deviation of 1D and 3D simulation results is less than 2% on a global scale.

6. Conclusion

Membrane distillation (MD) can be an important technology for desalting highly saline waters. DCMD is the simplest configuration form for MD processes, and is widely deployed in desalination processes, aqueous solution concentration for food industry applications and acid manufacturing. The efficiency and robustness of the numerical analysis used to obtain solutions for MD membranes and module problems such as temperatures, concentration polarizations, enhancement of the distillate fluxes etc. results in a wide application of CFD simulations as an analysis tool to study DCMD processes. CFD simulations can be coupled with other modelling/simulation software to provide interesting information to develop new DCMD membranes and modules. CFD models are very qualitative and in practice they can be helpful to select the best case and optimize the specific microstructure for membrane, spacer geometry and

Table 2
Applications, assumptions, utilized software, accuracy and finding results of the CFD models which reviewed at the section 4

References	Application	Assumption	Software
Al-Sharif et al. [61]	Performance investigation of three types of spacers (90°, 45° and 3 layer double ladder shaped non-woven spacers)	Constant heat flux through the membrane	Open Foam
Cipollina et al. [70]	Studying the effects of spacer and channel geometry to reduce temperature polarization at a spiral wound MD module channel	Simple reference geometry	ANSYS-CFX
Shakaib et al. [59]	Examining the effect of spacer orientation, inlet velocity and filament spacing on the shear stress distribution and temperature polarization in the MD modules	Constant thermal conductivity of the membrane material	ANSYS-Fluent
Yu et al. [88]	Studying the effect of the MD intrinsic mass transfer coefficient of the membrane to enhance the performance in both baffled and non-baffled modules	Laminar flow	ANSYS-Fluent
Yang et al. [60]	Investigating the effect of the microstructure of hollow fibers on the DCMD's performance	Geometry of the single fiber modules assumed to be ideal axially-symmetric structures Nine modified fibers assumed to have the similar membrane characteristics as the original fiber but with different surface geometries	ANSYS-Fluent
Katsandri [63,64]	Studying the effect of different hydrodynamic angles on the velocity profiles and shear stress Investigating how different inlet velocities and temperatures affect mass flux and temperature polarization	Fully permeable membrane	ANSYS-CFX
Yang et al. [83]	Analysis of the effect of turbulence promoters in hollow fiber membrane distillation modules	Geometry of the single fiber modules assumed to be ideal axially-symmetric structures Intrinsic mass transfer coefficient of the membrane assumed to be a constant	ANSYS-Fluent
Karode et al. [46]	Investigating of the pressure drop and shear rate of fluid flow through rectangular channels filled with several commercially available spacers for membrane modules	No-slip boundary condition is assumed to hold at all fluid–solid interfaces	PHOENICS CFD simulation package

Accuracy	Results
Good agreement in predicted velocity profiles compare to the experimental data.	Three layer, double ladder spacer improves the heat transfer and is the best performing spacer with the least pressure drop.
Some differences in predicted temperature profiles compare to the experimental data.	
No information provided.	Spacers can significantly affect temperature gradients within the channel, and modify the effective driving force between the faces of the membrane.
Simulated Nu values were in close agreement with the ones obtained from the experimental correlation.	Spacer orientation alters the temperature polarization and heat transfer rates. Temperature polarization is high in the arrangement where spacer filaments touch the top or bottom surfaces of membrane. Detached mode, the shear stress is higher and local values of temperature polarization index and shear stress are distributed more uniformly.
Simulation data agreed very well with the experimental values for mass fluxes. The relative errors were within $\pm 5\%$.	Increasing the intrinsic mass transfer coefficient value regardless of the existence of baffles decreases the temperature polarization coefficient. Increasing the operating temperature decreases the temperature polarization coefficient in the presence of a baffle. Raising the operating temperature had more effect on increasing the mass flux compared to application of baffles.
Good agreement with small relative errors of $\pm 5\%$ between CFD simulation results and experimental data of mass flux (N_m) and feed pressure drop (ΔP_f).	Wavy fiber shape the heat transfer coefficients were increased up to 4.5-fold while for the gear shape, there is an increase of approximately 5.5-fold. Average mass flux and temperature polarization coefficient of the gear shaped fiber module was enhanced 66% and 57%, respectively compared to the original straight fiber design.
CFD model predicted the experimental Nusselt number with a relative error $< 11\%$.	Optimal configuration is when the hydrodynamic angle $\alpha_f = 45^\circ$ as it produces better mixing, increases shear stress resulting in higher fluxes, and results in the highest mid-membrane temperature and temperature polarization coefficient. Least desirable configuration is when the hydrodynamic angle $\alpha_f = 0^\circ$, as this produces the lowest mid-membrane temperature and lowest temperature polarization coefficient.
Simulation results agreed very well with the experimental data. The relative errors were within $\pm 5\%$ for both mass flux and pressure drop results.	Applying the turbulence promoters resulted in slower decreasing trends along the fiber length for the feed heat-transfer coefficient (h_f) of the modified module compared to the original (unmodified) module. Temperature polarization coefficient and mass flux of the modified modules increased 57% and 74%, respectively. Attached quad spacers or floating round spacers can provide a good compromise between enhanced permeation fluxes and modest hydraulic energy consumption.
Good agreement with published experimental data at low inlet velocities ($< 0.5 \text{ m s}^{-1}$).	Spacers with equal filament diameters produce a higher pressure drop across the channel and these symmetric spacers also cause a more uniform shear rate at the top and bottom faces of the test cell.
Over predicted results compared to the published experimental data at higher inlet velocities.	Spacers with unequal filament diameters (asymmetric spacers) generated lower pressure drop and also resulted in an unequal shear rate on the top and bottom faces of the test cell.

the module geometry. The absence of significant industrial applications of the DCMD technology is partially because of the lack of proper module designing methods for which CFD simulation can be effective.

Most of the CFD work which studied DCMD processes has investigated the hydrodynamics and heat transfer in the channels of DCMD modules and spacer optimization in DCMD systems. However, a combination of these items with mass transfer should be investigated more extensively and comprehensively. Moreover, some of the physical phenomena which happen inside the membrane such as surface diffusion have been ignored in most of the CFD simulations which can be important when studying membrane synthesis and should be investigated further. Although CFD simulation can provide many advantages and opportunities for DCMD processes modelling, there are some critical concerns which should be investigated in future works. Due to the lack of proper module designing, there is the lack of significant industrial applications of the DCMD technology. Several of the recent CFD simulations focused on this issue; however as most of them extremely oversimplified the physical phenomena and the geometry, there is a room for further research. In addition, future 3D CFD modelling can include more complex mechanisms such as the permeable wall condition, fouling dynamics and multiple ionic component diffusion by incorporating user-developed routines to existing commercial and open-source CFD software packages.

Symbols

C	– Intrinsic mass-transfer coefficient of the membrane, $\text{kg m}^{-2} \text{s}^{-1} \text{Pa}^{-1}$
C_m	– Membrane constant, m^{-1}
L_x	– Interval between two corrugated waves on the membrane surface or interval between two insertions, mm
L_y	– Vertical distance between an internal and the membrane outer surface, mm
N_m	– Transmembrane mass flux, $\text{kg m}^{-2} \text{s}^{-1}$
Nu	– Nusselt number, –
P	– Pressure, Pa
r	– Radial direction in cylindrical coordinate, m
R_{mi}, R_{mo}	– Inner, outer radii of hollow fiber, m
Re	– Reynolds Number, –
T	– Temperature, K
u	– Normalized velocity of feed or permeate, ms^{-1}
u_{eff}	– Spacer effective velocity, ms^{-1}
ΔP	– Pressure drop, Pa
Δ_x	– Cross-sectional dimension of the regularly shaped internals or the wavy arch in the x direction, mm
Δ_y	– Cross-sectional dimension of the regularly shaped internals or the wavy arch in the r direction, mm
α_f	– Hydrodynamic angle/angle of attack, degree

Suffix

f	– Feed (subscript, superscript)
i, o	– Entrance, exit of the fluids

m	– Membrane (subscript)
p	– Permeate (subscript, superscript)

References

- [1] A. Alkhubdhiri, N. Darwish, N. Hilal, Membrane distillation: a comprehensive review, *Desalination*, 287 (2012) 2–18.
- [2] J. Koo, S. Lee, J.-S. Choi, T.-M. Hwang, Theoretical analysis of different membrane distillation modules, *Desal. Wat. Treat.*, 54 (2015) 862–870.
- [3] I. Hitsov, T. Maere, K. De Sitter, C. Dotremont, I. Nopens, Modelling approaches in membrane distillation: a critical review, *Sep. Purif. Technol.*, 142 (2015) 48–64.
- [4] A. Luo, N. Lior, Critical review of membrane distillation performance criteria, *Desal. Wat. Treat.*, 57 (2016) 20093–20140.
- [5] M. Gryta, K. Karakulski, A.W. Morawski, Purification of oily wastewater by hybrid UF/MD, *Water Res.*, 35 (2001) 3665–3669.
- [6] A. Criscuoli, E. Drioli, Energetic and exergetic analysis of an integrated membrane desalination system, *Desalination*, 124 (1999) 243–249.
- [7] H. Kurokawa, H. Sawa, Heat recovery characteristics of membrane distillation, *Heat Transfer Jpn. Res.*, 25 (1996) 135–150.
- [8] J. Blanco Gálvez, L. García-Rodríguez, I. Martín-Mateos, Seawater desalination by an innovative solar-powered membrane distillation system: the MEDESOL project, *Desalination*, 246 (2009) 567–576.
- [9] F.A. Banat, J. Simandl, Desalination by membrane distillation: a parametric study, *Sep. Sci. Technol.*, 33 (1998) 201–226.
- [10] C.-D. Ho, T.-J. Yang, Y.-C. Chuang, Performance improvement of countercurrent-flow direct contact membrane distillation in seawater desalination systems, *Desal. Wat. Treat.*, 51 (2013) 5113–5120.
- [11] M.A. Izquierdo-Gil, M.C. García-Payo, C. Fernández-Pineda, Air gap membrane distillation of sucrose aqueous solutions, *J. Membr. Sci.*, 155 (1999) 291–307.
- [12] P.P. Zolotarev, V.V. Ugrozov, I.B. Volkina, V.M. Nikulin, Treatment of waste water for removing heavy metals by membrane distillation, *J. Hazard. Mater.*, 37 (1994) 77–82.
- [13] G. Zakrzewska-Trznadel, M. Harasimowicz, A.G. Chmielewski, Concentration of radioactive components in liquid low-level radioactive waste by membrane distillation, *J. Membr. Sci.*, 163 (1999) 257–264.
- [14] V.D. Alves, I.M. Coelho, Orange juice concentration by osmotic evaporation and membrane distillation: a comparative study, *J. Food Eng.*, 74 (2006) 125–133.
- [15] S. Gunko, S. Verbych, M. Bryk, N. Hilal, Concentration of apple juice using direct contact membrane distillation, *Desalination*, 190 (2006) 117–124.
- [16] M.P. Godino, L. Peña, C. Rincón, J.I. Mengual, Water production from brines by membrane distillation, *Desalination*, 108 (1997) 91–97.
- [17] S.T. Hsu, K.T. Cheng, J.S. Chiou, Seawater desalination by direct contact membrane distillation, *Desalination*, 143 (2002) 279–287.
- [18] V. Calabro, B.L. Jiao, E. Drioli, Theoretical and experimental study on membrane distillation in the concentration of orange juice, *Ind. Eng. Chem. Res.*, 33 (1994) 1803–1808.
- [19] M. Tomaszewska, M. Gryta, A.W. Morawski, Study on the concentration of acids by membrane distillation, *J. Membr. Sci.*, 102 (1995) 113–122.
- [20] C. Huayan, W. Chunrui, J. Yue, W. Xuan, L. Xiaolong, Comparison of three membrane distillation configurations and seawater desalination by vacuum membrane distillation, *Desal. Wat. Treat.*, 28 (2011) 321–327.
- [21] Y. Yun, J. Wang, R. Ma, A.G. Fane, Effects of channel spacers on direct contact membrane distillation, *Desal. Wat. Treat.*, 34 (2011) 63–69.
- [22] J. Koo, J. Han, J. Sohn, S. Lee, T.-M. Hwang, Experimental comparison of direct contact membrane distillation (DCMD) with vacuum membrane distillation (VMD), *Desal. Wat. Treat.*, 51 (2013) 6299–6309.

- [23] K.W. Lawson, D.R. Lloyd, Membrane distillation, *J. Membr. Sci.*, 124 (1997) 1–25.
- [24] M.S. El-Bourawi, Z. Ding, R. Ma, M. Khayet, A framework for better understanding membrane distillation separation process, *J. Membr. Sci.*, 285 (2006) 4–29.
- [25] A.O. Imdakm, T. Matsuura, Simulation of heat and mass transfer in direct contact membrane distillation (MD): the effect of membrane physical properties, *J. Membr. Sci.*, 262 (2005) 117–128.
- [26] M. Khayet, A. Velázquez, J.I. Mengual, Modelling mass transport through a porous partition: effect of pore size distribution, *J. Non-Equilib. Thermodyn.*, 29 (2004) 279–299.
- [27] J. Phattaranawik, R. Jiraratananon, A.G. Fane, Effect of pore size distribution and air flux on mass transport in direct contact membrane distillation, *J. Membr. Sci.*, 215 (2003) 75–85.
- [28] L. Martínez, F.J. Florido-Díaz, A. Hernández, P. Prádanos, Estimation of vapor transfer coefficient of hydrophobic porous membranes for applications in membrane distillation, *Sep. Purif. Technol.*, 33 (2003) 45–55.
- [29] A.O. Imdakm, T. Matsuura, A Monte Carlo simulation model for membrane distillation processes: direct contact (MD), *J. Membr. Sci.*, 237 (2004) 51–59.
- [30] M. Khayet, N.N. Li, A.G. Fane, W.S. Winston Ho, *Membrane Distillation: Advance Membrane Technology and Applications*, John Wiley, New Jersey, USA, 2008.
- [31] M. Mulder, *Basic Principles of Membrane Technology*, Kluwer Academic Publishers, Netherlands, 2003.
- [32] M. Khayet, J.I. Mengual, G. Zakrzewska-Trznadel, Direct contact membrane distillation for nuclear desalination. Part I: review of membranes used in membrane distillation and methods for their characterisation, *Int. J. Nucl. Desalin.*, 1 (2005) 435–449.
- [33] C. Feng, B. Shi, G. Li, Y. Wu, Preparation and properties of microporous membrane from poly(vinylidene fluoride-co-tetrafluoroethylene) (F2.4) for membrane distillation, *J. Membr. Sci.*, 237 (2004) 15–24.
- [34] K.W. Lawson, M.S. Hall, D.R. Lloyd, Compaction of microporous membranes used in membrane distillation. I. Effect on gas permeability, *J. Membr. Sci.*, 101 (1995) 99–108.
- [35] J. Walton, H. Lu, C. Turner, S. Solis, H. Hein, *Solar and Waste Heat Desalination by Membrane Distillation*, College of Engineering, University of Texas at El Paso El Paso, Texas, USA, 2004.
- [36] A. Kullab, A. Martin, Membrane distillation and applications for water purification in thermal cogeneration plants, *Sep. Purif. Technol.*, 76 (2011) 231–237.
- [37] L.D. Nghiem, F. Hildinger, F.I. Hai, T. Cath, Treatment of saline aqueous solutions using direct contact membrane distillation, *Desal. Wat. Treat.*, 32 (2011) 234–241.
- [38] B.L. Pangarkar, S.K. Deshmukh, V.S. Sapkal, R.S. Sapkal, Review of membrane distillation process for water purification, *Desal. Wat. Treat.*, 57 (2016) 2959–2981.
- [39] K. Okiel, A.H.M. El-Aassar, T. Temraz, S. El-Etriby, H.A. Shawky, Vacuum enhanced direct contact membrane distillation for oil field produced water desalination: specific energy consumption and energy efficiency, *Desal. Wat. Treat.*, 57 (2016) 11945–11955.
- [40] P. Moghaddam Kamrani, O. Bakhtiari, P. Kazemi, T. Mohammadi, Theoretical modeling of direct contact membrane distillation (DCMD): effects of operation parameters on flux, *Desal. Wat. Treat.*, 56 (2015) 2013–2022.
- [41] G.A. Fimbres-Weihs, D.E. Wiley, Review of 3D CFD modeling of flow and mass transfer in narrow spacer-filled channels in membrane modules, *Chem. Eng. Process. Process Intensif.*, 49 (2010) 759–781.
- [42] H.K. Versteeg, W. Malalasekera, *An Introduction to Computational Fluid Dynamics: The Finite Volume Method*, Prentice Hall, London, 1995.
- [43] J.D. Anderson, G. Degrez, J. Degroote, E. Dick, R. Grundmann, J. Vierendeels, *Computational Fluid Dynamics: An Introduction*, 3rd ed., Springer, Berlin, 2009.
- [44] R. Ghidossi, D. Veyret, P. Moulin, Computational fluid dynamics applied to membranes: state of the art and opportunities, *Chem. Eng. Process. Process Intensif.*, 45 (2006) 437–454.
- [45] C.P. Koutsou, S.G. Yiantsios, A.J. Karabelas, Direct numerical simulation of flow in spacer-filled channels: effect of spacer geometrical characteristics, *J. Membr. Sci.*, 291 (2007) 53–69.
- [46] S.K. Karode, A. Kumar, Flow visualization through spacer filled channels by computational fluid dynamics I: pressure drop and shear rate calculations for flat sheet geometry, *J. Membr. Sci.*, 193 (2001) 69–84.
- [47] V.V. Ranade, A. Kumar, Fluid dynamics of spacer filled rectangular and curvilinear channels, *J. Membr. Sci.*, 271 (2006) 1–15.
- [48] F. Li, W. Meindersma, A.B. de Haan, T. Reith, Optimization of commercial net spacers in spiral wound membrane modules, *J. Membr. Sci.*, 208 (2002) 289–302.
- [49] M. Rahimi, S.S. Madaeni, K. Abbasi, CFD modeling of permeate flux in cross-flow microfiltration membrane, *J. Membr. Sci.*, 255 (2005) 23–31.
- [50] F. Banat, N. Jwaied, Economic evaluation of desalination by small-scale autonomous solar-powered membrane distillation units, *Desalination*, 220 (2008) 566–573.
- [51] R.B. Saffarini, E.K. Summers, H.A. Arafat, J.H. Lienhard V, Economic evaluation of stand-alone solar powered membrane distillation systems, *Desalination*, 299 (2012) 55–62.
- [52] S. Al-Obaidani, E. Curcio, F. Macedonio, G. Di Profio, H. Al-Hinai, E. Drioli, Potential of membrane distillation in seawater desalination: thermal efficiency, sensitivity study and cost estimation, *J. Membr. Sci.*, 323 (2008) 85–98.
- [53] S. Bouguecha, B. Hamrouni, M. Dhahbi, Small scale desalination pilots powered by renewable energy sources: case studies, *Desalination*, 183 (2005) 151–165.
- [54] Y.J. Choi, S. Lee, J. Koo, S.H. Kim, Evaluation of economic feasibility of reverse osmosis and membrane distillation hybrid system for desalination, *Desal. Wat. Treat.*, 57 (2016) 24662–24673.
- [55] A.M. Alkhalabi, N. Lior, Membrane-distillation desalination: status and potential, *Desalination*, 171 (2005) 111–131.
- [56] G.W. Meindersma, C.M. Guitj, A.B. de Haan, Desalination and water recycling by air gap membrane distillation, *Desalination*, 187 (2006) 291–301.
- [57] G. Zuo, R. Wang, R. Field, A.G. Fane, Energy efficiency evaluation and economic analyses of direct contact membrane distillation system using Aspen Plus, *Desalination*, 283 (2011) 237–244.
- [58] J. Blazek, *Computational Fluid Dynamics: Principles and Applications*, Elsevier B.V., Netherlands, 2015.
- [59] M. Shakaib, S.M.F. Hasani, I. Ahmed, R.M. Yunus, A CFD study on the effect of spacer orientation on temperature polarization in membrane distillation modules, *Desalination*, 284 (2012) 332–340.
- [60] X. Yang, H. Yu, R. Wang, A.G. Fane, Optimization of microstructured hollow fiber design for membrane distillation applications using CFD modeling, *J. Membr. Sci.*, 421–422 (2012) 258–270.
- [61] S. Al-Sharif, M. Albeirutty, A. Cipollina, G. Micale, Modelling flow and heat transfer in spacer-filled membrane distillation channels using open source CFD code, *Desalination*, 311 (2013) 103–112.
- [62] D.E. Wiley, D.F. Fletcher, Techniques for computational fluid dynamics modelling of flow in membrane channels, *J. Membr. Sci.*, 211 (2003) 127–137.
- [63] A. Katsandri, A theoretical analysis of a spacer filled flat plate membrane distillation modules using CFD: Part I: velocity and shear stress analysis, *Desalination*, 408 (2017) 145–165.
- [64] A. Katsandri, A theoretical analysis of a spacer filled flat plate membrane distillation modules using CFD: Part II: temperature polarisation analysis, *Desalination*, 408 (2017) 166–180.
- [65] Z. Xu, Y. Pan, Y. Yu, CFD simulation on membrane distillation of NaCl solution, *Front. Chem. Eng. China*, 3 (2009) 293–297.
- [66] H. Yu, X. Yang, R. Wang, A.G. Fane, Numerical simulation of heat and mass transfer in direct membrane distillation in a hollow fiber module with laminar flow, *J. Membr. Sci.*, 384 (2011) 107–116.

- [67] M. Shakaib, S.M.F. Hasan, M. Mahmood, CFD modeling for flow and mass transfer in spacer-obstructed membrane feed channels, *J. Membr. Sci.*, 326 (2009) 270–284.
- [68] J. Schwinge, D.E. Wiley, D.F. Fletcher, A CFD study of unsteady flow in narrow spacer-filled channels for spiral-wound membrane modules, *Desalination*, 146 (2002) 195–201.
- [69] Z. Cao, D.E. Wiley, A.G. Fane, CFD simulations of net-type turbulence promoters in a narrow channel, *J. Membr. Sci.*, 185 (2001) 157–176.
- [70] A. Cipollina, A. Di Miceli, J. Koschikowski, G. Micale, L. Rizzuti, CFD simulation of a membrane distillation module channel, *Desal. Wat. Treat.*, 6 (2012) 177–183.
- [71] T. Echekki, E. Mastorakos, *Turbulent Combustion Modeling: Advances, New Trends and Perspectives*, Springer, New York, USA, 2011.
- [72] V. Yakhot, S.A. Orszag, Renormalization group analysis of turbulence. I. Basic theory, *J. Sci. Comput.*, 1 (1986) 3–51.
- [73] B.E. Launder, D.B. Spalding, *Mathematical Models of Turbulence*, Academic Press, New York, USA, 1972.
- [74] T.-H. Shih, W.-W. Liou, A. Shabbir, Z. Yang, J. Zhu, A new $k-\epsilon$ eddy viscosity model for high Reynolds number turbulent flows, *Comput. Fluids*, 24 (1995) 227–238.
- [75] K. Myrillas, A. Gosset, P. Rambaud, J.M. Buchlin, CFD simulation of gas-jet wiping process, *Eur. Phys. J. Spec. Top.*, 166 (2009) 93–97.
- [76] F.R. Menter, Two-equation eddy-viscosity turbulence models for engineering applications, *AIAA J.*, 32 (1994) 1598–1605.
- [77] D.A. Johnson, L.S. King, A mathematically simple turbulence closure model for attached and separated turbulent boundary layers, *AIAA J.*, 23 (1985) 1684–1692.
- [78] T.J. Chung, *Computational Fluid Dynamics*, Cambridge University Press, University of Alabama in Huntsville, 2002.
- [79] ANSYS-FLUENT, ANSYS Inc., Canonsburg, PA, USA, 2017.
- [80] C. Meneveau, J. Katz, Scale-invariance and turbulence models for large-eddy simulation, *Annu. Rev. Fluid Mech.*, 32 (2000) 1–32.
- [81] P.A.V. Olivares, *Acoustic Wave Propagation and Modeling Turbulent Water Flows with Acoustics for District Heating Pipes*, Uppsala University, Uppsala, 2009.
- [82] V.V. Ranade, A. Kumar, Comparison of flow structures in spacer-filled flat and annular channels, *Desalination*, 191 (2006) 236–244.
- [83] X. Yang, H. Yu, R. Wang, A.G. Fane, Analysis of the effect of turbulence promoters in hollow fiber membrane distillation modules by computational fluid dynamic (CFD) simulations, *J. Membr. Sci.*, 415–416 (2012) 758–769.
- [84] M. Shakaib, S.M.F. Hasani, M. Ehtesham-ul Haque, I. Ahmed, R.M. Yunus, A CFD study of heat transfer through spacer channels of membrane distillation modules, *Desal. Wat. Treat.*, 51 (2013) 3662–3674.
- [85] A. Cipollina, G. Micale, L. Rizzuti, Membrane distillation heat transfer enhancement by CFD analysis of internal module geometry, *Desal. Wat. Treat.*, 25 (2011) 195–209.
- [86] J. Phattaranawik, R. Jiraratananon, A.G. Fane, Heat transport and membrane distillation coefficients in direct contact membrane distillation, *J. Membr. Sci.*, 212 (2003) 177–193.
- [87] M.M.A. Shirazi, A. Kargari, M.J.A. Shirazi, Direct contact membrane distillation for seawater desalination, *Desal. Wat. Treat.*, 49 (2012) 368–375.
- [88] H. Yu, X. Yang, R. Wang, A.G. Fane, Analysis of heat and mass transfer by CFD for performance enhancement in direct contact membrane distillation, *J. Membr. Sci.*, 405–406 (2012) 38–47.
- [89] J. Seo, Y.M. Kim, J.H. Kim, Spacer optimization strategy for direct contact membrane distillation: shapes, configurations, diameters, and numbers of spacer filaments, *Desalination*, 417 (2017) 9–18.
- [90] J. Zhu, L. Jiang, T. Matsuura, New insights into fabrication of hydrophobic/hydrophilic composite hollow fibers for direct contact membrane distillation, *Chem. Eng. Sci.*, 137 (2015) 79–90.
- [91] Z. Song, L. Li, H. Wang, B. Li, S. Wang, DCMD flux curve characteristics of cross-flow hollow fiber membrane, *Desalination*, 323 (2013) 107–113.
- [92] M.M.A. Shirazi, A. Kargari, A.F. Ismail, T. Matsuura, Computational fluid dynamic (CFD) opportunities applied to the membrane distillation process: state-of-the-art and perspectives, *Desalination*, 377 (2016) 73–90.
- [93] G. Naidu, S. Jeong, S. Vigneswaran, Interaction of humic substances on fouling in membrane distillation for seawater desalination, *Chem. Eng. J.*, 262 (2015) 946–957.
- [94] S. Goh, J. Zhang, Y. Liu, A.G. Fane, Membrane distillation bioreactor (MDBR) – a lower green-house-gas (GHG) option for industrial wastewater reclamation, *Chemosphere*, 140 (2015) 129–142.
- [95] S. Goh, Q. Zhang, J. Zhang, D. McDougald, W.B. Krantz, Y. Liu, A.G. Fane, Impact of a biofouling layer on the vapor pressure driving force and performance of a membrane distillation process, *J. Membr. Sci.*, 438 (2013) 140–152.
- [96] M. Gryta, The assessment of microorganism growth in the membrane distillation system, *Desalination*, 142 (2002) 79–88.
- [97] M. Krivorot, A. Kushmaro, Y. Oren, J. Gilron, Factors affecting biofilm formation and biofouling in membrane distillation of seawater, *J. Membr. Sci.*, 376 (2011) 15–24.
- [98] S.A. Adcock, J.A. McCammon, Molecular dynamics: survey of methods for simulating the activity of proteins, *Chem. Rev.*, 106 (2006) 1589–1615.
- [99] M. Karplus, J.A. McCammon, Molecular dynamics simulations of biomolecules, *Nat. Struct. Biol.*, 9 (2002) 646.
- [100] S.J. Marrink, A.H. de Vries, D.P. Tieleman, Lipids on the move: simulations of membrane pores, domains, stalks and curves, *Biochim. Biophys. Acta, Biomembr.*, 1788 (2009) 149–168.
- [101] M. Herzberg, M. Elimelech, Biofouling of reverse osmosis membranes: role of biofilm-enhanced osmotic pressure, *J. Membr. Sci.*, 295 (2007) 11–20.
- [102] M.B. Boudinar, W.T. Hanbury, S. Avlonitis, Numerical simulation and optimisation of spiral-wound modules, *Desalination*, 86 (1992) 273–290.
- [103] A. Katsandri, *An Experimental and CFD Theoretical Study of Enhancing Mass Flux in Flat Plate Direct Contact Membrane Distillation*, Reading University, Reading, UK, 2011.
- [104] A.R. Da Costa, A.G. Fane, D.E. Wiley, Spacer characterization and pressure drop modelling in spacer-filled channels for ultrafiltration, *J. Membr. Sci.*, 87 (1994) 79–98.
- [105] S. Srisurichan, R. Jiraratananon, A.G. Fane, Mass transfer mechanisms and transport resistances in direct contact membrane distillation process, *J. Membr. Sci.*, 277 (2006) 186–194.
- [106] G. Rao, S.R. Hiibel, A.E. Childress, Simplified flux prediction in direct-contact membrane distillation using a membrane structural parameter, *Desalination*, 351 (2014) 151–162.
- [107] K.W. Lawson, D.R. Lloyd, Membrane distillation. II. Direct contact MD, *J. Membr. Sci.*, 120 (1996) 123–133.
- [108] B. Haddadi, C. Jordan, M. Miltner, M. Harasek, Membrane modeling using CFD: Combined evaluation of mass transfer and geometrical influences in 1D and 3D, *J. Membr. Sci.*, 563 (2018) 199–209.